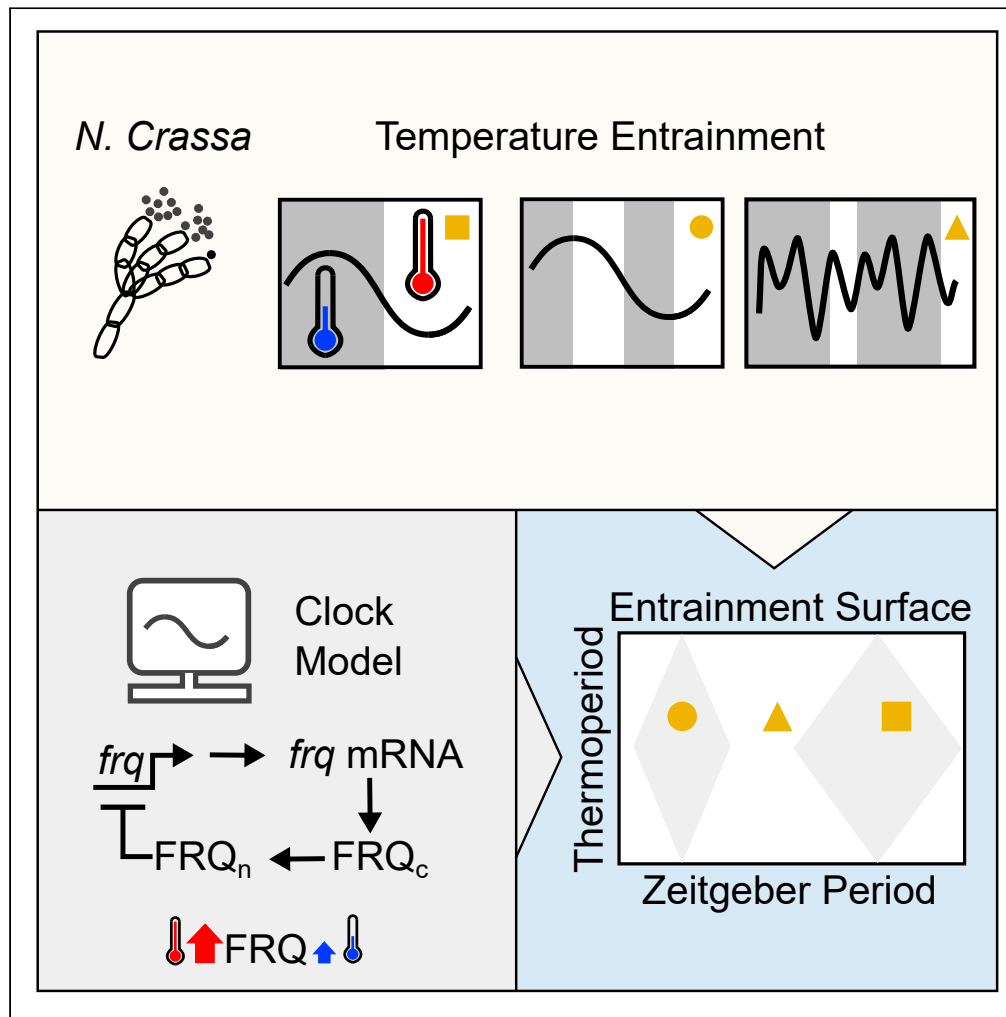


Article

Principles underlying the complex dynamics of temperature entrainment by a circadian clock



Philipp Burt,
Saskia Grabe,
Cornelia Madeti,
..., Till
Roenneberg,
Hanspeter Herzog,
Christoph Schmal

christoph.schmal@hu-berlin.de

Highlights

Temperature cycles can entrain the fungal model organism *Neurospora crassa*

We study the circadian surface for 99 combinations of τ , T and thermoperiod

1:1 entrainment, period doubling and other non-linear phenomena are observed

A mathematical model of temperature entrainment explains the observed complexity



Article

Principles underlying the complex dynamics of temperature entrainment by a circadian clock

Philipp Burt,^{1,2,5} Saskia Grabe,^{1,2,5} Cornelia Madeti,^{3,5} Abhishek Upadhyay,^{1,2,4} Martha Merrow,³ Till Roenneberg,³ Hanspeter Herzel,^{1,2} and Christoph Schmal^{1,2,6,*}

SUMMARY

Autonomously oscillating circadian clocks resonate with daily environmental (zeitgeber) rhythms to organize physiology around the solar day. Although entrainment properties and mechanisms have been studied widely and in great detail for light-dark cycles, entrainment to daily temperature rhythms remains poorly understood despite that they are potent zeitgebers. Here we investigate the entrainment of the chronobiological model organism *Neurospora crassa*, subject to thermocycles of different periods and fractions of warm versus cold phases, mimicking seasonal variations. Depending on the properties of these thermocycles, regularly entrained rhythms, period-doubling (frequency demultiplication) but also irregular aperiodic behavior occurs. We demonstrate that the complex nonlinear phenomena of experimentally observed entrainment dynamics can be understood by molecular mathematical modeling.

INTRODUCTION

From its outset, life on Earth is confronted with rhythmic changes in environmental conditions such as day and night, tides or seasons. To cope with daily changes of light and temperature, many organisms have evolved an autonomous circadian clock that rhythmically controls both behavior and physiology. A fundamental property of circadian clocks is that under physiological conditions, they entrain to an external zeitgeber such as light, food intake or temperature. By this means, physiological processes such as immune responses, metabolic activity or behavior are aligned rhythmically across the day. Thus, properties of zeitgeber cycles drive the evolution of the entire circadian system and it has been shown that geophysical differences in light conditions drive genetically encoded latitudinal clines of clock properties (Rosato et al. (1996); Sawyer et al. (1997); Hut et al. (2013)). In humans, misalignment between the clock and the external environment has been associated with cancer, diabetes and inflammatory diseases (Fuhr et al. (2015)). In plants, it leads to a decrease in photosynthesis and growth (Dodd et al. (2005)). The intricate regulation of the clock and its modulation by external stimuli requires a thorough understanding of generic clock principles. A rhythmic zeitgeber together with the intrinsic circadian clock it affects, constitutes a system of coupled periodic oscillators (Balanov et al. (2009)). Oscillator theory and mathematical modeling have proven to be useful tools for the investigation of circadian rhythms as they allow for a systematic study of entrainment parameters such as the occurrence of synchronization, entrainment amplitudes or entrainment phases ψ in dependence on the underlying zeitgeber and clock properties (Wever (1979)). For example, a prediction is that relatively short intrinsic periods τ lead to early entrainment phases (Wever (1965); Pittendrigh and Daan (1976)).

The filamentous fungus *Neurospora crassa* has been widely used as a circadian model organism in the past decades (Hurley et al. (2016)). *Neurospora crassa* has a fully sequenced genome and because of its haploid life cycle it is possible to perform genetic screens without backcrossing. In its asexual life cycle *Neurospora* produces visible spores, so-called conidia, which can be quantified by densitometric analysis (Belden et al. (2007)). Pioneered by Goldbeter and Ruoff, the transcriptional feedback loop that leads to circadian rhythms of *Neurospora* has been modeled mathematically (Leloup et al. (1999); Ruoff et al. (2001); Francois (2005)). In particular, the role of protein degradation and mechanisms of temperature and glucose compensation have been studied in detail (Ruoff et al. (2005); Dovzhenok et al. (2015); Upadhyay et al. (2019)). More recently, oscillator theory has been applied to explore entrainment by light of different *Neurospora* strains (Rémi et al. (2010); Bordyugov et al. (2015)).

¹Institute for Theoretical Biology, Faculty of Life Sciences, Humboldt-Universität zu Berlin, Unter den Linden 6, 10117 Berlin, Germany

²Institute for Theoretical Biology, Charité Universitätsmedizin Berlin, Charitéplatz 1, 10117 Berlin, Germany

³Institute of Medical Psychology, Faculty of Medicine, LMU Munich, Goethestrasse 31, 80336 Munich, Germany

⁴Friedrich Miescher Institute for Biomedical Research, Maulbeerstrasse 66, 4058 Basel, Switzerland

⁵These authors contributed equally

⁶Lead contact

*Correspondence: christoph.schmal@hu-berlin.de

<https://doi.org/10.1016/j.isci.2021.103370>



On the molecular level, self-sustained rhythms in *Neurospora* are generated by a delayed negative feedback loop with the frequency protein FRQ as the key element. The cycle starts with the transcription of the frequency gene (*frq*) driven by the heterodimer WCC, composed of the subunits WC-1 and WC-2. After a delay that is controlled by multiple phosphorylations and complex formations, FRQ protein inhibits its own transcription, thus closing the negative feedback loop which ultimately leads to autonomous circadian rhythmicity (Aronson et al. (1994); Dunlap (1999); Lee et al. (2000); Schafmeier et al. (2005); Larrondo et al., 2015; Upadhyay et al. (2020)). Notably, although light entrainment has been studied in *Neurospora* in detail both on the behavioral and molecular level, entrainment through temperature changes has received less attention (Rémi et al. (2010); Crosthwaite et al. (1995); Liu et al. (1997, 1998); Mellow et al. (1999); Rensing and Ruoff (2002); Lee et al. (2003)).

Here, we systematically explore the entrainment behavior of three different *Neurospora* strains (one wild type and two *frq* mutants), exposed to temperature cycles of up to five different lengths (T cycles). The combination of T cycles with a wild type strain, a short period mutant and a long period mutant created a dense network of τ - T relationships which would allow a granular understanding of the relationship of endogenous period to phase of entrainment. Furthermore, we varied the relative duration of the warm phase (27°C) with respect to the cold phase (22°C) of a zeitgeber cycle, ranging from 16% to 84% in 9 steps. In this way, we mimicked photoperiods with temperature cycles, further probing entrainment with various temporal structures. Alterations in zeitgeber structure can change the effective zeitgeber strength. Thus, the experimental design invites a thorough analysis of entrainment.

Using a combination of experiment and mathematical modeling, we address the following questions: What is the range of entrainment under varying conditions? Are there nonlinear phenomena outside of the 1:1 entrainment range? Do we find the expected association of the mismatch between τ and T and phase of entrainment (ψ)? How do seasonal environmental variations affect entrainment?

We find an astonishing complexity within the experimental recordings including 1:2 entrainment, superposition of two frequencies (tori), and reproducible aperiodic behavior that resembles deterministic chaos. Moreover, using a simple biophysically motivated molecular model of the temperature entrained *Neurospora crassa* core clock, we show that almost all observations including the aperiodic behavior can be explained by a single periodically driven oscillator.

RESULTS

Neurospora crassa shows complex patterns of conidiation rhythms upon temperature entrainment

Circadian rhythms are generated at the single cell level through gene regulatory networks. Quantification of gene expression oscillations can be labor intensive and costly. Thus, more indirect measures from circadian clock controlled processes such as stem elongation and leaf movement rhythms in plants (Mayer (1966)) or behavioral activity rhythms in mammals (Johnson (1926)) and flies (Konopka and Benzer (1971)) are commonly used to deduce properties of the underlying circadian clock, such as the free-running period τ or phase of entrainment ψ , being defined as the phase difference between the circadian clock and a given reference point along the zeitgeber cycle. Here, we use densitometrically analyzed patterns of *N. crassa* conidia formation on agar medium, plated in glass tubes ('race tube assays'), as a proxy for circadian clock properties. To investigate mechanisms of temperature entrainment, we systematically exposed different strains of *N. crassa* to thermocycles of three different T cycles, namely $T = 16\text{h}$, 22h , and 26h . All experiments were constructed using cycles of 22°C a 27°C which corresponds to a zeitgeber amplitude of 2.5°C. In each series of T cycles, nine different thermoperiods namely $x_T = 0.16, 0.25, 0.33, 0.4, 0.5, 0.6, 0.67, 0.75, 0.84$ were tested. Thermoperiods are defined as the fraction $x_T = \frac{W}{W+C}$ of the cycle length occupied by the warm phase W , where the cold phase is $C = T - W$. In $T = 12\text{h}$ and $T = 24\text{h}$, entrainment was investigated at a reduced set of three different thermoperiods $x_T = 0.25, 0.5, 0.75$ and $x_T = 0.16, 0.25, 0.33$, respectively.

Qualitative changes in the dynamical behavior of conidiation rhythms occurred for variations in zeitgeber structures and endogenous period according to the underlying *N. crassa* strain (Figure 1). For example, the wild type (*frq*⁺) strain with a free-running period of $\tau \approx 22\text{h}$ in constant conditions robustly entrains to an equinoctial thermocycle ($x_T = 0.5$) of period $T = 22\text{h}$ that closely matches the period of the internal clock (Figure 1A). Transient dynamics approaching the entrained state (see first two days of Figure 1A) are

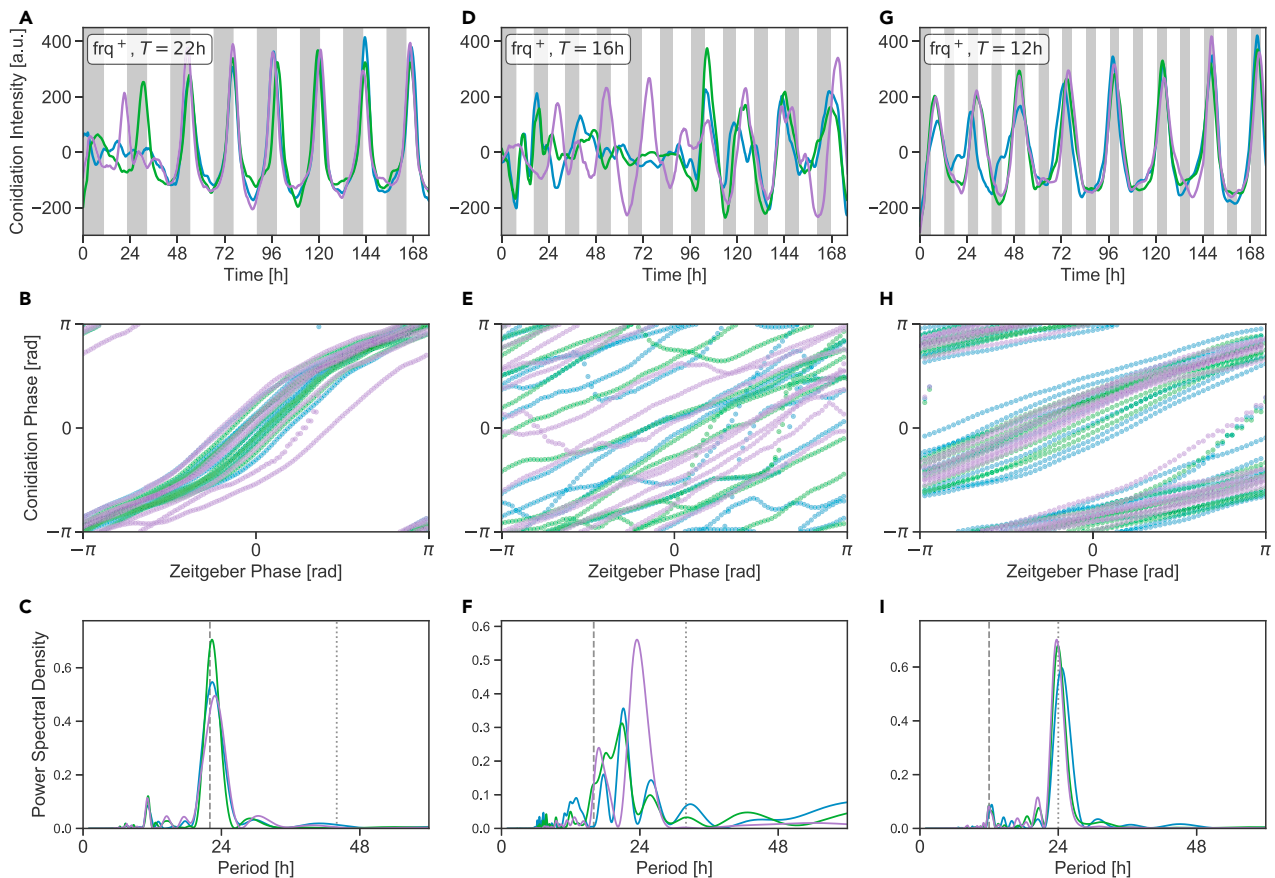


Figure 1. Complex dynamics upon temperature entrainment

(A–C) Robust 1:1 entrainment can be observed for the frq^+ strain under temperature cycles of $T = 22\text{h}$ with 50% warm phase ($x_T = 0.5$). This is reflected in the densitometrically quantified time traces of conidiation patterns (A), in the phase locked dynamics between the zeitgeber and conidiation cycle (B) and in the spectrum of the corresponding oscillations as quantified by a Lomb-Scargle periodogram (C).

(D–F) Conidiation patterns of the frq^+ strain do not entrain to a $T = 16\text{h}$ thermocycle of $x_T = 0.5$.

(G–I) Frequency demultiplication or 2:1 entrainment can be observed in rhythmic conidiation patterns of the frq^+ strain, subject to $T = 12\text{h}$ thermocycles of thermoperiod $x_T = 0.5$.

Different colors in panels (A–I) indicate technical replicates under the same experimental condition. Gray bars denote cold phases (22°C) while white background indicates warm phases (27°C). Dashed gray lines denote the zeitgeber period T while dotted gray lines denote a period of $2T$ in panels (C), (F) and (I).

indicative of an entrainment effect as opposed to a simple coincidence between free-running and zeitgeber periods. In addition to a visual inspection of the raw time series data, we use two classical approaches from the theory of nonlinear dynamics to classify the state of entrainment, i.e., (1) by relating the time-dependent (instantaneous) phase of oscillatory conidiation pattern with the corresponding zeitgeber signal (see Figure S1 for a detailed introduction) and (2) a detailed inspection of the the oscillations power spectrum as obtained by a Lomb-Scargle analysis (Bergé et al. (1984); Schuster (1994)). Here, instantaneous phases as estimated by a Hilbert transformation, suggest entrainment, i.e., the conidiation cycle progresses by 2π (or 360°) along a full zeitgeber cycle which leads to single confined bands in Figure 1B. Dominant peaks close to the zeitgeber period in the corresponding Lomb-Scargle spectrograms suggest frequency locking between the thermocycle and conidiation rhythms (Figure 1C).

Conidiation patterns fail to entrain if the period of an equinoctial ($x_T = 0.5$) thermocycle is reduced to $T = 16\text{h}$, 6h shorter than the frq^+ strain's internal free-running period of $\tau \approx 22\text{h}$ (Figure 1D). No systematic dependency between the instantaneous phases of the zeitgeber cycles and the conidiation patterns was observed (Figure 1E). Lack of entrainment is further reflected in the corresponding Lomb-Scargle periodogram (Figure 1F), showing no agreement between the dominant spectral peaks and the entrainment period T .

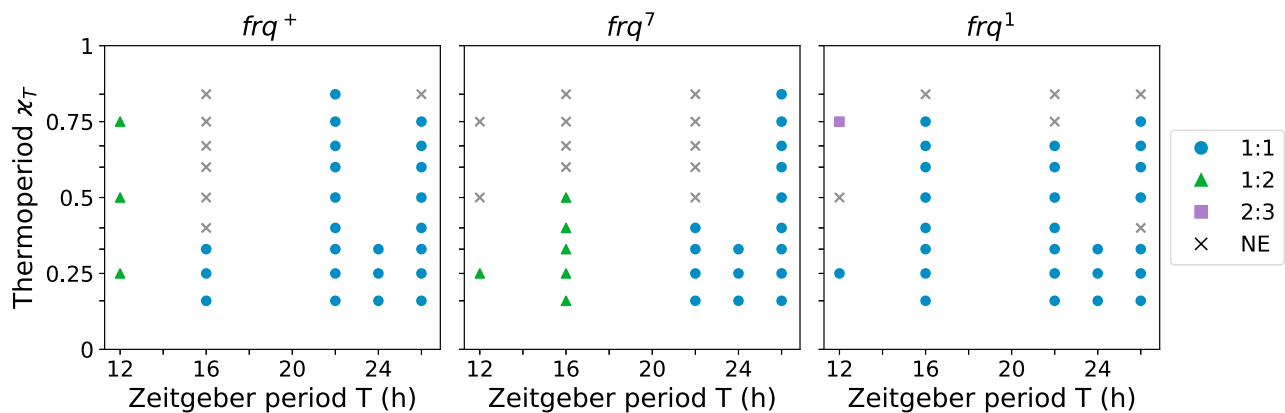


Figure 2. Circadian surface for temperature entrainment

Overview on *Neurospora crassa* conidiation experiments for wild type frq^+ (left), long period mutant frq^7 (middle), and short period mutant frq^1 (right) strains, exposed to varying temperature cycle length (T ; x axis) and thermoperiods (x_T ; y axis). Each data point represents one experimental condition. Occurrence of entrainment has been analyzed by inspecting raw data, phase plots and spectral decomposition via Lomb-Scargle periodograms, see Figures S2–S10. 1:1 entrainment is represented by circles, 1:2 entrainment by triangles, 2:3 entrainment by squares, and conditions where no entrainment (NE) occurs by crosses.

A further reduction of the T cycle to $T = 12$ h, close to half of the frq^+ strains internal free-running period, again leads to robust entrainment (Figures 1G and 1H). Here, one cycle of conidiation occurs every second full thermocycle, leading to a conidiation period of approximately $2T = 24$ h, see Figure 1I, a phenomenon, commonly known as frequency demultiplication (Bruce (1960); Roenneberg et al. (2005)) or 1:2 entrainment (Pikovsky et al. (2001)). The observed frequency multiplication dynamics for $T = 12$ h, $x_T = 50\%$ using the frq^+ strain (Figure 1G) closely match results of a corresponding experiment as previously reported in (Morrow et al. (1999)) and can thus serve as a positive control for further experiments as described below.

We classified experimentally observed dynamics under temperature entrainment for all 99 different combinations of the three different strains, five different entrainment periods and up to nine different thermoperiods, using a semi-automated approach (Figure 2). The observed dynamics are grouped into four categories, namely non-entrained, 1:1, 1:2 and 2:3 entrained oscillations (compare Figures S2–S10).

Modeling temperature entrainment

To investigate the underlying principles of the experimentally observed complexity in temperature entrainment, we exploit a detailed mathematical model of the *Neurospora crassa* core clock as previously published (Hong et al. (2008); Hong Model). The Hong model has been curated to explain rhythmic oscillations of core clock genes frq and $wc-1$ in the wild type (WT) and the two mutant strains (frq^+ , frq^1 and frq^7 , respectively) in constant darkness. Figure 3A shows a schematic representation of the regulatory network. It consists of seven ordinary differential equations (ODEs) and 17 parameters (Equation 1 and Table 1 in STAR Methods show the detailed model structure and its corresponding kinetic parameters).

Although WC-1 and WC-2 have been shown to be involved in light entrainment (Froehlich et al. (2002); Liu (2003)), molecular details underlying temperature entrainment remain less understood. However, FRQ has been described to oscillate at a higher magnitude and amplitude with increasing temperatures (Liu et al. (1998)), potentially through alternative splicing of frq mRNA (Diernfellner et al. (2005); Colot et al. (2005); Diernfellner et al. (2007)). Similar to other organisms, *Neurospora crassa* shows temperature compensation of its circadian free-running period (Gardner and Feldman (1981)). To reveal parameters that reproduce these features upon temperature impact, we applied a comprehensive sensitivity and bifurcation analysis of the Hong model (Figures S11 and S12, respectively). As a result, changes in frq transcription and frq translation rates (parameters k_1 and k_2 , respectively) are found to mimic temperature induced changes in amplitude while, the free-running period remains largely stable. Based on these qualitative observations, we constructed a conceptual model of temperature entrainment by assuming that temperature changes affect the clock by modulating the transcription rate k_1 of frq mRNA. We later elaborate in section Discussion similarities and differences that arise by implementing the effect of temperature through modulations

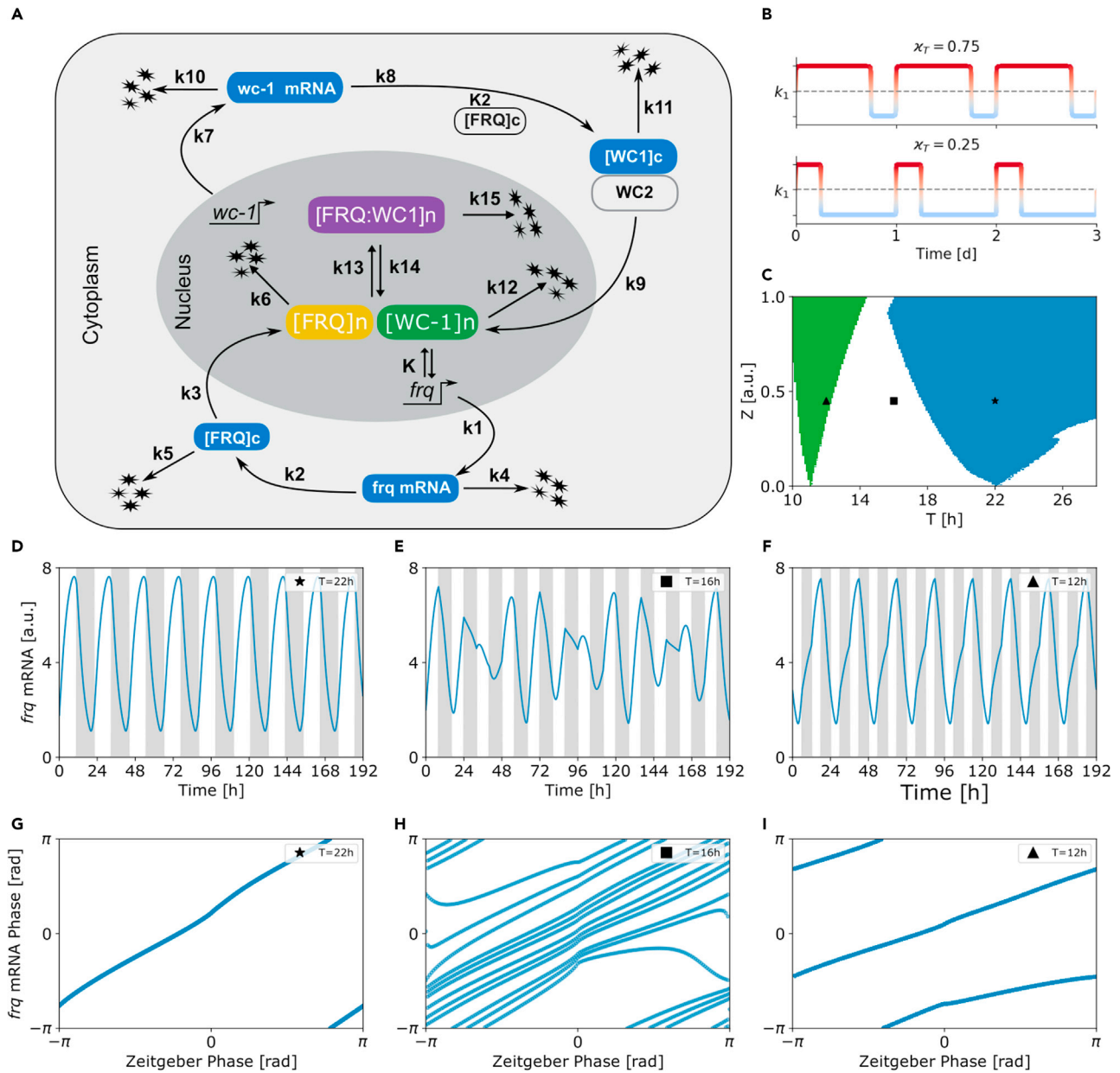


Figure 3. Different synchronization regimes (Arnold tongues) within a molecular clock model are able to explain the complex dynamics of *Neurospora* temperature entrainment

(A) Schematic drawing of the regulatory network underlying the *Hong model* (adapted from (Hong et al. (2008); Upadhyay et al. (2019))).

(B) Sketch of the temperature cycle induced regulation of the maximal transcription rate as described in STAR Methods for two different thermoperiods x_T . For a given zeitgeber strength z_0 , the rate fluctuates between $k_1 - \frac{x_T}{2}k_1$ and $k_1 + \frac{x_T}{2}k_1$ around its nominal value of k_1 . Phases of hot and cold temperatures are denoted by red and blue colors, respectively.

(C) 1:1 (blue) and 2:1 (green; frequency demultiplication) synchronization regions (Arnold tongues) in the *Hong model*, entrained by equinoctial square wave temperature cycles as given by Equations 4 and 5.

(D–F) Illustrative, representative example simulations of *frq* mRNA dynamics for equinoctial ($x = 0.5$) temperature cycles at three different periods $T = 22\text{h}$, $T = 16\text{h}$, and $T = 12\text{h}$, respectively, at a constant zeitgeber strength of $z_0 = 0.45$.

(G–I) Instantaneous phases of *frq* mRNA dynamics of sub-panels (D–F), plotted against corresponding zeitgeber phases. Parameter values corresponding to results plotted in sub-panels (D–I) have been highlighted by different markers in sub-panel (B), respectively.

Table 1. Kinetic parameters of the *Hong model*

Description	Parameter	Value (h^{-1})
<i>frq</i> transcription	k_1	1.80
<i>frq</i> mRNA translation	k_2	1.80
Import to nucleus	k_3	0.05
<i>frq</i> mRNA degradation	k_4	0.23
Degradation	k_5	0.27
Degradation	k_6	0.07
<i>wc-1</i> transcription	k_7	0.16
<i>wc-1</i> mRNA translation (dependent)	k_8	0.80
Import to nucleus	k_9	40.00
<i>wc-1</i> mRNA degradation	k_{10}	0.10
Degradation	k_{11}	0.05
Degradation	k_{12}	0.02
Complex formation	k_{13}	50.00
Complex dissociation	k_{14}	1.00
Complex degradation	k_{15}	5.00
Binding to <i>frq</i> -promoter	K	1.25
mRNA complex formation	K_2	1.00

of parameter k_2 for which variations lead to an almost identical change in amplitude and period of *frq* oscillations.

Periodically driven limit cycle oscillator models explain complex entrainment behaviors

To approximate experimentally applied temperature cycles, we use square-wave-like zeitgeber signals (see Equations 4 and 5 of STAR Methods and Figure 3B) such that parameter k_1 is modulated between $k_1 + \frac{z_0}{2}k_1$ and $k_1 - \frac{z_0}{2}k_1$ for warm and cold temperatures in dependence on zeitgeber strength z_0 , respectively. Upon this, the *Hong model* shows typical hallmarks of entrainment (Pikovsky et al. (2001)). It can be easily entrained to zeitgeber signals with a period (T) close to the internal free-running period (τ). For increasing zeitgeber strength z_0 , the clock is able to entrain to a broader range of zeitgeber periods T , leading to tongue shaped entrainment region in the $z_0 - T$ parameter plane, called the *Arnold tongue* (Arnold (1987)), see blue area in Figure 3C. Within this tongue, 1:1 synchronization similar to the behavior of the *frq*⁺ strain under equinoctial temperature cycles of $T = 22\text{h}$ occurs (Figures 1A, 1B, 3D, and 3G).

Entrainment not only occurs for zeitgeber periods close to the free-running period τ . Higher order synchronization is generally possible at rational fractions $\frac{n}{m}$ ($n:m$ entrainment) where n is the number of cycles to which the internal clock adheres during m cycles of the zeitgeber signal (Balanov et al. (2009)), as illustrated for the 1:2 entrainment region (frequency demultiplication) of the *Hong model* in Figure 3C (green). Graphs F, and I correspond to dynamics observed for the *frq*⁺ strain under equinoctial temperature cycles of $T = 12\text{h}$ (compare Figures 1G and 1H). The entrainment regions or *Arnold tongues* become smaller with increasing synchronization order (Figure 3C) as predicted from the literature.

Driving a single self-sustained oscillator by an external zeitgeber can result in an astonishing complexity of qualitatively different dynamics that can go beyond the synchronized patterns described above (Heltberg et al. (2021)). Even in the absence of synchronization (absolute coordination) outside the *Arnold tongues* where no period- or phase-locking occurs, the zeitgeber is still able to affect the oscillations of the internal clock, a phenomenon called relative coordination (v. Holst (1938)). In this dynamical regime, complex phenomena leading to non-periodic dynamics (Figures 3E and 3H) as, e.g., observed for the *frq*⁺ strain under equinoctial temperature cycles of $T = 16\text{h}$ (compare Figures 1G and 1H) are characteristic.

The qualitatively different dynamics that can arise outside the *Arnold tongues* depend on oscillator properties as well as zeitgeber strength (z_0) and period (T) and are thus informative about the underlying structure of the system. Here, we vary z_0 and T to systematically investigate dynamics outside the entrainment

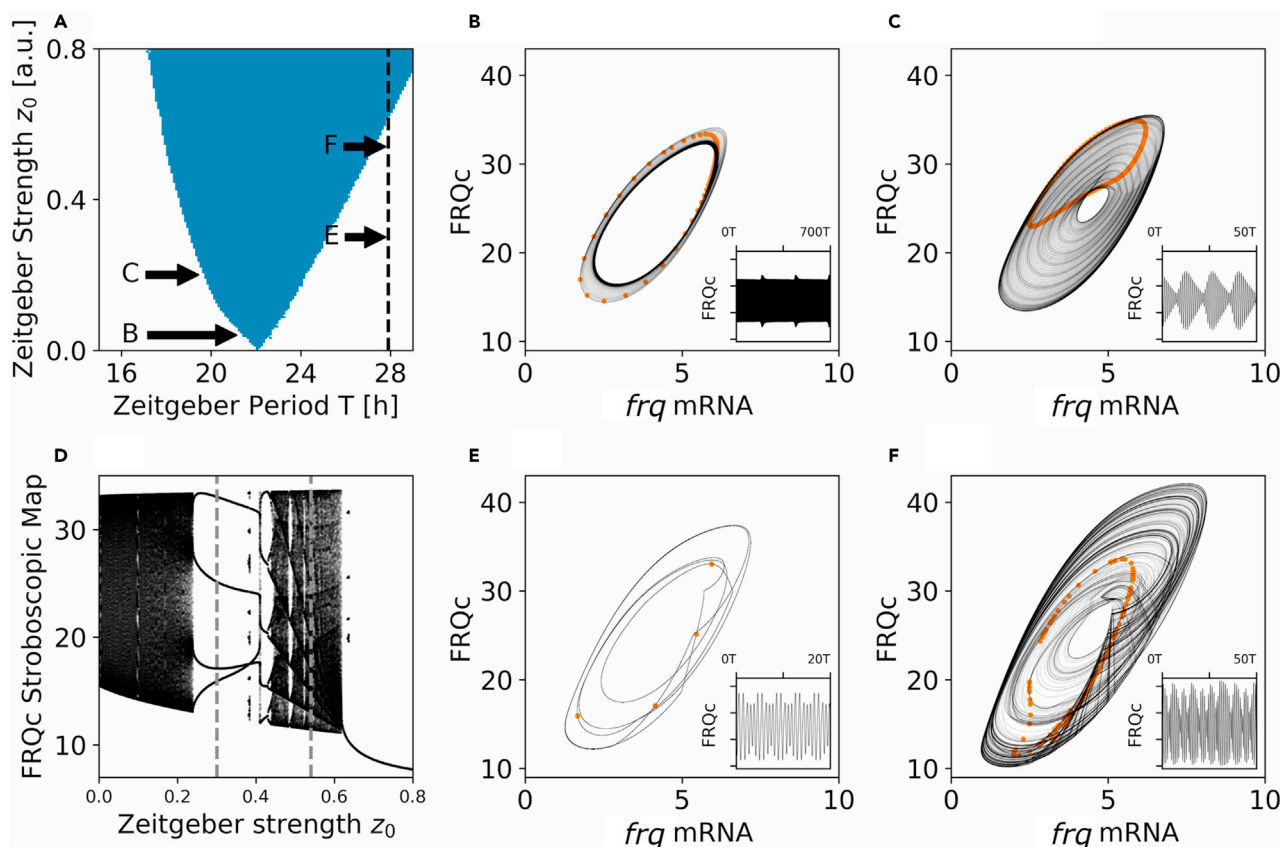


Figure 4. Complex dynamical behavior is observed outside the entrainment range

- (A) 1:1 synchronization region (Arnold tongue, blue) in the Hong model, entrained by a thermoperiod of $\tau_T = 0.75$. Combinations of z_0 and T underlying panels (B), (C), (E) and (F) are indicated by arrows. Range of z_0 at $T = 27.9$ h underlying panel (D) is depicted by a dashed vertical line.
- (B) Projection of a trajectory from the Hong model showing slow amplitude modulations for zeitgeber strength $z_0 = 0.04$ and period $T = 21.37$ h in the frq mRNA and cytosolic FRQ protein (FRQc) plane, after decay of transient dynamics. Orange dots show the associated stroboscopic map. Inset shows corresponding FRQc dynamics over the time of 700 entrainment periods T .
- (C) Same as (B) showing beating behavior for $z_0 = 0.2$ and $T = 19.58$ H
- (D) One-parameter diagram of values from the FRQc stroboscopic map versus different zeitgeber strength z_0 .
- (E) Same as (B) showing n:m higher order synchronization behavior for $z_0 = 0.3$ and $T = 27.9$ H
- (F) Same as (B) showing chaotic behavior for $z_0 = 0.54$ and $T = 27.9$ H

region within the *Neurospora* circadian clock (Figure 4). Close to the borders of entrainment, right after leaving the entrainment regime, two types of slow modulations of the intrinsic oscillations typically emerge (Balanov et al. (2009); Granada et al. (2011)). At relatively low zeitgeber strength (z_0) long-period amplitude modulations occur (Figure 4B inset). These are characterized by a torus in phase space (Figure 4B) and a spectrum containing a peak at the period of the zeitgeber signal, a peak at the internal period of the circadian clock as well as peaks at combinations of these two periods (Figure S13, Balanov et al. (2009)). Another common approach to classify dynamics of an externally driven dynamical system is to investigate its stroboscopic map (a special case of the more general Poincaré map) which can be defined for a one-dimensional time series by a set of points, taken at the fixed interval of the entrainment period T . In case of amplitude modulations this stroboscopic map forms a closed curve (Figure 4B orange dots, Balanov et al. (2009); Granada et al. (2011)). As one gets closer to the entrainment region, the modulation period (i.e., period of the amplitude envelope) lengthens tremendously, whereas the diameter of the stroboscopic map remains relatively constant (Figure S13). At higher zeitgeber strength (z_0) beating is observed, i.e., the superposition of two frequencies, again characterized by a torus in phase space and a closed curve for the stroboscopic map (Figure 4C). Characteristically, the beating period lengthens and, in contrast to amplitude modulations for lower zeitgeber strength, the diameter of the stroboscopic map reduces while the spectral peak associated with the internal circadian period becomes smaller as one approaches the limits of

entrainment (Figure S14, Balanov et al. (2009)). In case of amplitude modulations and beating and in contrast to synchronized dynamics, the ratio $\frac{n}{m}$, with n being the number of internal clock cycles per m cycles of the zeitgeber signal, is not a rational number and the phase difference of both signals *slips* or *drifts* over time (Bergé et al. (1984); Heltberg et al. (2021)). These dynamics are typically known as quasi-periodic.

By systematically investigating the dynamics for different zeitgeber strength (z_0) at a given period (T) using the stroboscopic map of cytosolic FRQ protein (FRQc) oscillations, a collection of qualitatively different dynamics can be observed (Figures 4D–4F). With increasing zeitgeber strength (z_0) at $T = 27.9\text{h}$, the system evolves from quasiperiodic torus oscillations through a couple of higher order synchronization regimes (e.g. Figure 4E) until it reaches another qualitatively different dynamical regime, i.e., chaotic behavior (e.g. Figure 4F), before entering the 1:1 entrainment region (*Arnold tongue*) at $z_0 \approx 0.62$ (compare also Figure S15 for an illustration). Chaotic oscillations can be characterized by a large sensitivity to initial conditions such that even two arbitrarily close starting points will exponentially diverge while being still bounded to a confined region in phase space that is spanned by the systems dynamical variables (Bergé et al. (1984); Schuster (1994)). Such chaotic dynamics exhibit apparently unpredictable dynamics with randomly fluctuating amplitudes (Figure 4F, *inset*), small “bumps” within the stroboscopic map (Figure 4F) and broad backgrounds in their power spectra (Figure S15, Bergé et al. (1984); Schuster (1994); Heltberg et al. (2021)).

In summary, fundamental synchronization properties of a limit cycle oscillator such as the *Hong model*, when entrained to a periodic forcing signal, explain the complex patterns of conidiation rhythms that have been observed under equinoctial ($\kappa = 0.5$) temperature entrainment in the wild type *Neurospora crassa* strain (compare similarities in Figures 1 and 3). Apart from 1:1 and 1:2 synchronization patterns, we find non-periodic irregular oscillation with randomly fluctuating amplitudes, similar to those found in some experimental conidiation experiments (e.g., 1 D). Even though experimental time series are too short to formally proof, this could suggest the existence of non-autonomous chaotic dynamics in the driven *Neurospora* clock, indicating that the system is in a strongly driven regime.

In the next section we extend this analysis to the full circadian surface, i.e. all combinations of zeitgeber periods T and thermoperiods κ_T as summarized in Figure 2A.

Simulated clock dynamics are able to explain behavior across the full circadian surface of the *frq*⁺ wild type strain

Temperature entrained conidiation rhythms of the wild type *Neurospora crassa* strain (*frq*⁺) show different dynamical regimes, depending on zeitgeber period (T) and thermoperiod (κ_T ; Figure 2A). 1:1 entrainment is observed when T is close to $\tau \approx 22\text{h}$, 1:2 entrainment occurs when T is around 50% of τ , and non-entrained dynamics occur when $T = 16\text{h}$ and $T = 26\text{h}$. Especially for short zeitgeber periods of $T = 16\text{h}$, the *frq*⁺ strain entrains better under short thermoperiods at the experimentally chosen zeitgeber amplitude.

For an arbitrarily chosen zeitgeber strength z_0 , most of the simulated clock dynamics ($\sim 50\%$ in Figure 5A) do not agree with experimentally observed conidiation rhythms. The location, width, and tilt of the *Arnold onions* (synchronization regimes, Schmal et al. (2015)) is determined by both properties of the internal clock and the external zeitgeber. Although the width of the Arnold onion is determined by multiple factors such as, e.g., the strength of the zeitgeber signal or the amplitude and radial relaxation rate of the circadian clock, the position of the entrainment regions in the $\kappa_T - T$ plane is mainly determined by the clock's internal free-running period τ . In autonomous dynamical systems such as the *Hong model*, the internal free-running period τ can always be rescaled while keeping other oscillatory properties such as the amplitude and waveform unaltered, see STAR Methods. Along these lines, we searched for minimal modifications of our conceptual temperature entrainment model to better mimic experimental findings. To this end, we exhaustively investigated different combinations of internal periods τ and external zeitgeber strengths z_0 for their fit of the data (Figure 5B). We fitted the entrainment state of the data for each of the 33 combinations of zeitgeber period T and thermoperiod κ_T , i.e. we asked whether a non-entrained, 1:1 entrained or 1:2 entrained dynamics was observed and compared this with the dynamics described in Figure 2.

It turns out that scaling of free-running τ and zeitgeber strength z_0 is sufficient for an “optimal” fit, i.e. all entrainment states of the experiment can be reproduced by simulation (Figures 5B and 5C). To mimic the experimentally observed 1:2 entrainment at $T = 12\text{h}$, slightly longer values of τ_{opt} in comparison to the 22h free-running period under constant darkness of the *Hong model* emerge (Figure 5B; stars).

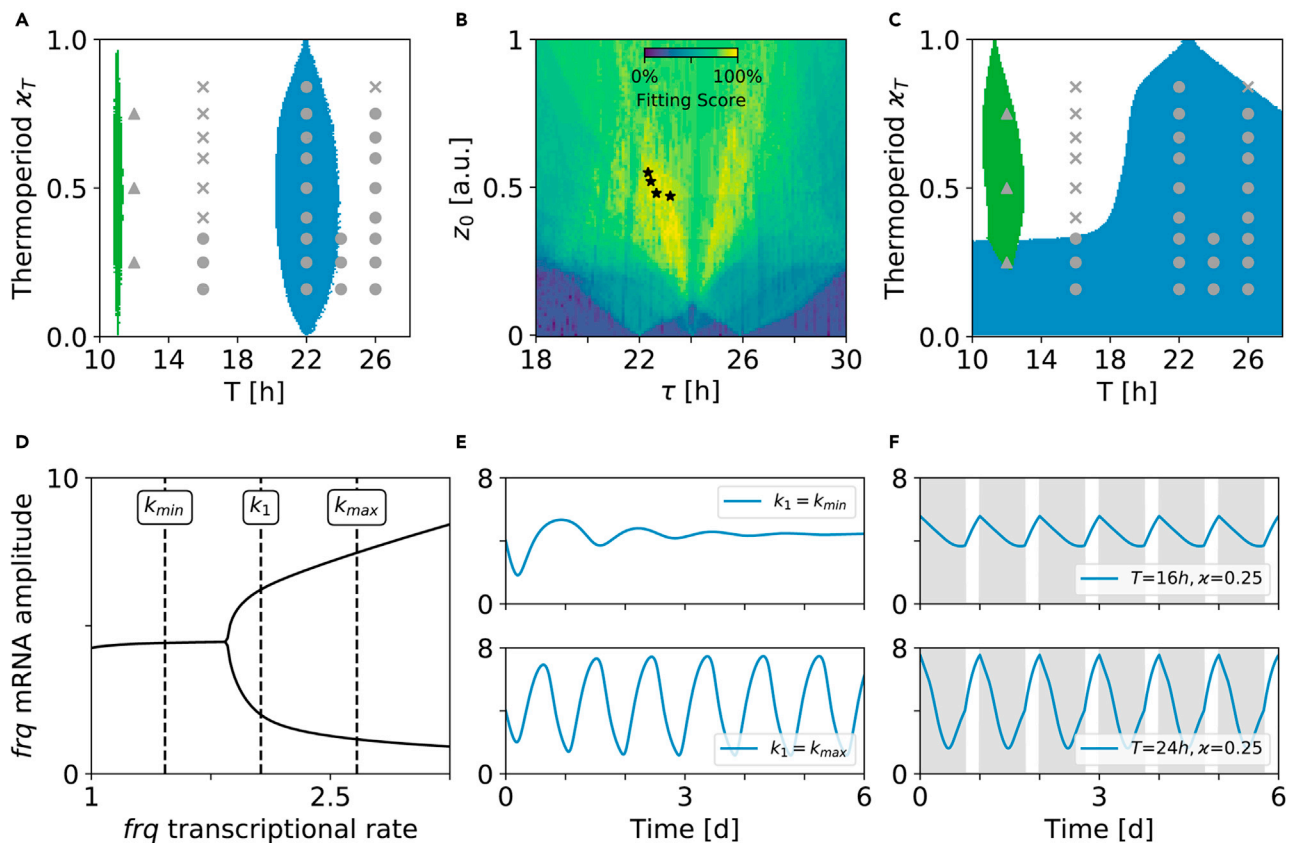


Figure 5. Good agreement of experimental and simulated wild type (*frq*⁺) *Neurospora crassa* entrainment dynamics after proper scaling of the models free running period and zeitgeber strength

(A) Experimentally observed dynamics (gray symbols) together with simulated 1:1 (blue) and 2:1 (green; frequency demultiplication) synchronization regions in the thermoperiod - zeitgeber period parameter plane (Arnold onions). A zeitgeber strength of $z_0 = 0.1$ and the nominal parameter set of the *Hong model* (see Table 1) have been used.

(B) Fitting scores for different zeitgeber strength z_0 and scaled internal free-running periods τ . The fitting score in percent denotes the fraction of simulated dynamics that qualitatively matches the experimentally observed ones, i.e. whether 1:1 entrainment, 2:1 frequency-demultiplication or unentrained dynamics are observed. Stars denote parameter combinations that lead to a fitting score of 100%.

(C) Experimentally observed entrainment dynamics and simulated synchronization regions (Arnold onions) as in panel (A) for an exemplary "optimal" parameter combination of panel (B), namely $z_0 = 0.47$ and $\tau \approx 23.19$ h.

(D) Bifurcation diagram, showing the qualitative changes of the modified *Hong model* from panel (C) for variations in the *frq* transcriptional rate k_1 that mediate alterations in temperature variations within our modeling approach. Depicted are the minimum and maximum values of *frq* mRNA oscillations. A single bold line for $k_1 \leq 1.56$ corresponds to a stable steady state, whereas the two bold lines for $k_1 \geq 1.56$ correspond to peak and trough values of self-sustained *frq* mRNA oscillations. Vertical dashed line marked by k_1 denotes the nominal parameter value while vertical dashed lines marked by k_{min} and k_{max} denote temperature-modulated k_1 values at 22°C and 27°C for $z_0 = 0.47$ and $\tau \approx 23.19$ h as in panel (C), respectively.

(E) Simulated *frq* mRNA dynamics under constant temperatures at 22°C (i.e. $k_1 = k_{min}$; top) and 27°C (i.e., $k_1 = k_{max}$; bottom).

(F) *frq* mRNA dynamics under $\chi_T = 0.25$ short-thermoperiod entrainment conditions at zeitgeber periods of $T = 16$ h (top) and $T = 24$ h (bottom).

Interestingly, our fit leads to values that are in accordance with the experimentally observed free-running period and inter-individual period heterogeneity (Diegmann et al. (2010)).

Damped oscillations at cold temperatures facilitate entrainment under short thermoperiods

At zeitgeber period $T = 16$ h, experimental conidiation rhythms entrain at short thermoperiods for $\chi_T = 0.16, 0.25, 0.33$ but failed to entrain at longer thermoperiods. This behavior is not reproducible with the onion shaped entrainment region of a weakly forced circadian system as shown in Figure 5A. Instead, "optimal" fits lead to a 1:1 entrainment region that widens under short thermoperiods (Figure 5C). This widening can be explained by qualitatively different dynamical behaviors of the modified *Hong model* when subjected to constant cold versus constant warm temperatures (Figure 5D). For low temperatures that lead to values of $k_1 < 1.56$, the system shows damped oscillations that approach a constant steady state

after the decay of transients (e.g., Figure 5E top). With increasing constant temperatures the system eventually reaches a critical threshold $k_c \approx 1.56$ at which self-sustained oscillations emerge with smoothly growing amplitudes for increasing temperatures (Figures 5D and 5E bottom). Such qualitative changes upon parameter variations are termed bifurcations in dynamical systems theory. The particular bifurcation described above, which leads to self-sustained oscillations from a stable steady state, is known as Hopf bifurcation. Interestingly, modeling and experimental evidence suggests that the post-translational oscillator of the cyanobacteria circadian clock undergoes a similar Hopf bifurcation, leading to damped oscillations under cold temperatures (Murayama et al. (2017)).

Damped oscillators (such as the physical pendulum with friction) typically synchronize more easily by an external force in comparison to self-sustained pacemakers (Bain et al. (2004); Gonze et al. (2005); Murayama et al. (2017)). At low thermoperiods $\kappa_T < 0.5$, the system is driven into the damped oscillatory regime for most part of the day which in turn leads to a facilitated entrainment for a broad range of zeitgeber periods that ultimately leads to a broadening of the Arnold onion toward shorter thermoperiods as observed in Figure 5C. In contrast, for large thermoperiods $\kappa_T > 0.5$, the system resides within the self-sustained oscillatory regime for the larger part of the entrainment cycle that is typical for a driven self-sustained oscillator as observed in Figure 5A and discussed in (Schmal et al. (2015; 2020)). A similar broadening of the entrainment region has been recently observed for a light-entrained *Goodwin* oscillator under long photoperiods (Ananthasubramaniam et al. (2020)).

It should be noted, that though entrainment of damped oscillators is generally possible for large ranges of zeitgeber periods T , common resonance effects such as amplification of amplitudes are typically stronger for zeitgeber periods close to the intrinsic free-running period τ . Interestingly, a corresponding behavior can be found in our simulations (Figure 5F) as well as experimentally observed conidiation patterns (Figure S2) at low thermoperiods.

Predicted correlations between ψ , κ_T and T are supported by experiment

In the case of synchronization, a stable phase relation between the zeitgeber signal and the internal clock, commonly termed the phase of entrainment ψ , emerges. A proper phase of entrainment is of fundamental importance as it ensures that diurnal physiological processes are aligned at appropriate times around the day. Figure 6A shows simulated entrainment phases ψ of cytosolic FRQ protein (FRQc) oscillations at different thermoperiods κ_T and two different zeitgeber periods $T = 22\text{h}$ and $T = 26\text{h}$, corresponding to the phases along vertical cross-sections through Figure 5C. The two periods correspond to those experimentally investigated periods showing the largest fraction of 1:1 entrained conidiation rhythms across varying thermoperiods in the *frq*⁺ strain. Simulations predict later phases of entrainment ψ with increasing thermoperiods κ_T and decreasing zeitgeber periods T (Figure 6A). For $T = 26\text{h}$ the shift of ψ toward later phases with increasing κ_T saturates and reaches a plateau after $\kappa_T \geq 0.5$. The dependencies of the entrainment phase ψ on κ_T and T are qualitatively similar to the corresponding behavior in temperature entrained conidiation patterns. Analogous to simulated 1:1 entrained FRQc oscillations, conidiation rhythms of the *frq*⁺ strain show consistently later phases with decreasing zeitgeber period T and in most cases a monotonic increase of ψ with increasing thermoperiod κ_T (Figures 6B–6D). To the best of our knowledge, this is the first demonstration that variations in thermoperiods tune the phase of entrainment in *Neurospora crassa* in a similar way than photoperiods.

DISCUSSION

Circadian entrainment has been predominantly studied using light as a synchronizing cue. Entrainment to temperature cycles has attracted less attention even though circadian clocks have been shown to synchronize to thermocycles of surprisingly low amplitudes such as 1 – 2°C in poikilotherms (Hoffmann (1969); Wheeler et al. (1993); Somers et al. (1998); Rensing and Ruoff (2002)) or tissue cultures of homeotherms (Brown et al. (2002); Abraham et al. (2010); Buhr et al. (2010)). In the present paper we find diverse and complex dynamical responses during the entrainment of circadian *Neurospora crassa* conidiation rhythms subject to temperature cycles and subsequently show that this complexity can be well understood by mathematical models of molecular regulatory networks underlying the intracellular circadian clock.

Entrainment of oscillatory systems generally depends on properties of the intrinsic oscillator as well as the periodic stimulation. We analyzed these differential contributions by systematically varying the period T and thermoperiod κ_T in temperature entrainment experiments using three different *Neurospora crassa*

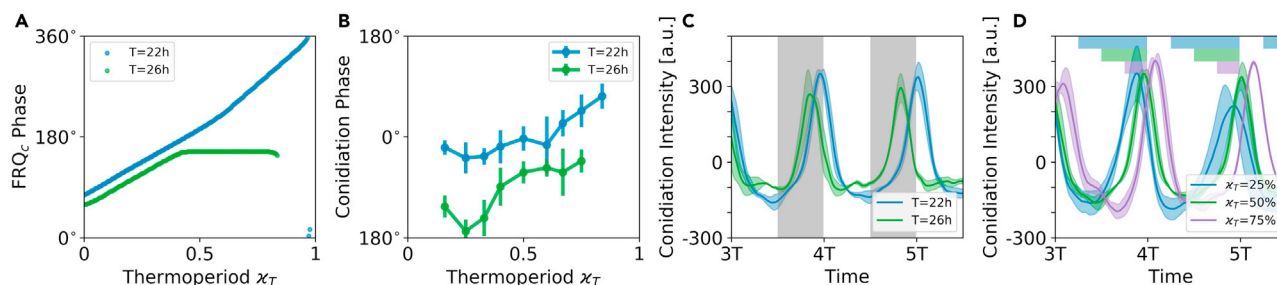


Figure 6. Earlier phases in longer entrainment cycles and later phases for increasing thermoperiods are observed in experiment and simulation

(A) Simulated entrainment phases of the *Hong model*, determined by a peak picking method on simulated FRQ_c oscillations, for parameters as in Figure 5C under different thermoperiods x_T and two different zeitgeber periods, namely $T = 22h$ (blue) and $T = 26h$ (green).

(B) Entrainment phases determined from 1:1 synchronized conidiation patterns of the frq^+ strain upon $T = 22h$ (blue) and $T = 26h$ (green) entrainment cycles, using a peak-picking method. Each data point represents the circular mean and standard deviation, determined from all detected oscillation peaks (acrophases) of all three replicates at a given x_T and T . Peaks from the first three entrainment cycles have been neglected as transients.

(C) Exemplary 1:1 synchronized conidiation patterns under equinoctial temperature entrainment of period $T = 22h$ (blue) and $T = 26h$ (green) show the behavior as expected from simulations, namely earlier phases for longer entrainment cycles.

(D) Analogously to panel (C), exemplary 1:1 synchronized conidiation patterns under $T = 22h$ show earlier phases for shorter thermoperiods x_T as expected from simulations of the *Hong model*. As in Figures 1 and 3, phases of entrainment have been defined using the onset of the warm period as a reference point, i.e. 0° or 360° refer to the transition from cold to warm temperatures. Gray shaded areas in panel C denote periods of cold temperatures. Colored bars at the top of panel D denote periods of cold temperatures under different thermoperiods. Bold lines on panels C-D denote averages, whereas the transparent areas denote standard deviations of all three conidiation pattern replicates of the frq^+ strain as found in Figure S2.

strains with different intrinsic circadian periods τ . Although the wild type frq^+ and the long period frq^7 strains consistently show regular 1:1 entrainment only for zeitgeber periods that are relatively close to their previously published intrinsic free running periods, short period mutant frq^1 is generally able to entrain to a broader range of T - x_T combinations. This is consistent with experimental findings, reporting substantially smaller amplitudes of FRQ oscillations for the frq^1 in comparison to the frq^+ and frq^7 strains (Huang et al. (2006)) as small oscillation amplitudes lead to large amplitude PRCs and thus broader entrainment ranges (Lakin-Thomas et al. (1991); Schmal et al. (2015)). Higher order 1:2 synchronization also known as frequency demultiplication can be observed at zeitgeber periods close to 50% of the strains intrinsic period ((Merrow et al. (1999)), Figure 2). Such a behavior has been analogously shown for light-entrained conidiation rhythms of *Neurospora crassa* (Rémi et al. (2010)). Noteworthy, the wild type frq^+ and long period frq^7 strains generally entrain better to short thermoperiods in comparison to long thermoperiods, being in contrast to the previously theoretically predicted symmetrical behavior for conceptual amplitude-phase oscillator models (Schmal et al. (2015); Diekman and Bose (2018)). Outside the synchronization regimes, we observe differently pronounced non-entrained and irregular behavior, characterized by drifting phases with respect to zeitgeber signals or fluctuating instantaneous periods and amplitudes.

To study principles underlying the experimentally observed complex entrainment behaviors, we employed a previously published detailed ordinary-differential-equation based mathematical model (Hong et al. (2008)) that considers the main regulatory interactions of the *Neurospora crassa* core clock. By using a detailed sensitivity and bifurcation analysis of the model parameters, constrained by experimentally observed behaviors such as temperature compensation (Gardner and Feldman (1981)) and the higher baseline expression and oscillation amplitude of FRQ protein at higher temperatures (Liu et al. (1998)), we suggest variations in frq transcription and translation rates as a potential driver underlying temperature entrainment. Although this approach differs from the common assumption that changes in temperature affect all kinetic parameters, often modeled via Arrhenius equations (Ruoff et al. (2005); Tseng et al. (2012)), it reduces the number of necessary parameters tremendously and thus facilitates the model analysis and interpretation.

Using variations in frq transcriptional rate as a mechanism of temperature entrainment, we varied the intrinsic free-running period (τ) and zeitgeber strength (z_0) and qualitatively compared the simulated entrainment states with the experimentally observed dynamics. This is tantamount to fitting the synchronization regimes (i.e., *Arnold tongues* and *Arnold onions*) to experimental data in the zeitgeber period T and thermoperiod x_T parameter plane. Similar approaches have been previously used to understand, for example, entrainment behavior of cardiac cells (Guevara et al. (1981); Glass et al. (1984)) or photoperiodic

entrainment of plant circadian clocks (De Caluwe et al. (2017)). In summary, the qualitative synchronization behavior can be reproduced for all experimentally tested combinations of T and x_T in the frq^+ wild type strain. Our unbiased optimization approach led to free-running periods τ , close to those that have been experimentally observed. Thus, the dependencies between synchronization regimes and free-running periods as predicted from oscillator theory (Balanov et al. (2009); Pikovsky et al. (2001)) are reproduced by our experiments. It should be noted that adiabatic variations of (constant) frq mRNA translation rate k_2 show an almost identical impact on frq amplitudes and periods, thus being an alternative candidate in mediating the impact of temperature onto clock dynamics. Applying an identical optimization protocol as described above reveals that, indeed, temperature entrainment via k_2 leads to similar results, compare Figures 5, 6A, and S16. Similar to k_1 entrainment, k_2 -mediated temperature entrainment reaches an almost perfect (32 out of 33 experimentally observed entrainment dynamics) optimization score (Figure S16A), yields a similarly shaped entrainment region in the $x_T - T$ parameter plane (Figure S16B) and adopts qualitatively similar (Figure S16C), yet slightly earlier (Figures S16D and S16E) entrainment phases of FRQ_c oscillations.

For conceptual (amplitude-phase) oscillator models, we have previously shown that entrainment regions in the zeitgeber period and photoperiod parameter plane adopt an onion-shaped geometry, called *Arnold onions* (Schmal et al. (2015; 2020)). We find the same geometrical structure for the entrainment region in case of the detailed molecular *Hong model* (Figure 5A). The 1:1 synchronization region has its widest entrainment range at the equinox and tapers toward zeitgeber periods (T) that correspond to the circadian clock's internal free-running period τ for increasingly extreme thermoperiods ($x_T \approx 0$ or $x_T \approx 1$). For photo-periodic entrainment, a tilt of this onion-shape geometry is expected, because free-running periods often differ under constant darkness and constant light, known as Aschoff's rule (Aschoff (1958)). In contrast, such a tilt is not expected in case of temperature entrainment because of temperature compensation of free-running period τ , a behavior that is faithfully mimicked by the temperature entrained *Hong model* (Figure 5A, blue).

Our optimization approach predicts that the experimentally observed broader entrainment regime for short thermoperiods relies on the bifurcation structure of the *Neurospora crassa* circadian clock. Bifurcations are qualitative changes of systems dynamics because of changes in a certain parameter. Here, our optimization based modeling approach predicts that the circadian clock of *Neurospora crassa* moves from a self-sustained to a damped oscillatory regime for increasingly cold temperatures which ultimately leads to a broad entrainment range under short thermoperiods as damped oscillators can be more easily entrained. Interestingly, this is in line with experimental observations, showing an increasing damping and lowering amplitudes among conidiation patterns for decreasing temperatures (Liu et al. (1997)). Above described entrainment behavior at low thermoperiods could be a general phenomenon among non-homeothermic organisms as damped circadian rhythms under cold temperatures have been described for several other poikilotherms such as cockroaches (Roberts (1960)), fruit flies (Zimmerman (1969); Maguire et al. (2014)), or plants (Bünning and Tazawa (1957)). In addition, the circadian clock of the post-translational oscillator of cyanobacteria has been shown to undergo a Hopf bifurcation with decreasing temperatures that leads to damped oscillations (Murayama et al. (2017)), similar to the behavior observed in our modeling study (Figure 5D). It would be interesting to investigate whether the characteristic entrainment behavior with a broadening entrainment range at low thermoperiods as found in our experimental and simulation studies (Figures 2 and 5C) can be similarly observed among those organisms, or, to systematically investigate experimentally whether the *Neurospora* circadian clock undergoes a Hopf bifurcation for decreasing temperatures similar to the findings in cyanobacteria (Murayama et al. (2017)).

Simulations of the modified *Hong model* subject to temperature cycles reveal qualitatively different dynamics between the synchronization regimes. Close to the limits of entrainment typically beating and modulations (tori) were observed, similar to results from conceptual amplitude-phase models (Balanov et al. (2009); Granada et al. (2011)). Between successive higher-order synchronization regimes, we identified regions of chaotic dynamics, analogous to what has been found in other molecular circadian clock models subject to light entrainment (Gonze and Goldbeter (2000); De Caluwe et al. (2017)). Such non-autonomous chaotic behavior resembles the experimentally observed irregular aperiodic conidiation patterns with randomly fluctuating amplitudes in the absence of synchronization (e.g. Figure 1D), suggesting that the temperature entrained *Neurospora* circadian clock is rather a strongly driven system. However, it should be noted that the existence of chaos cannot be formally proven within the relatively short recordings of

our experiments (Bradley and Kantz (2015)). It would be interesting to repeat experiments at the $x_T - T$ parameter combinations that are predicted to show chaotic behaviors, using experimental techniques that allow substantially longer time series recordings.

In conclusion, our study reveals complex temperature entrainment behavior for *Neurospora crassa* conidiation rhythms including higher order synchronization and nonlinear phenomena such as chaos or quasiperiodicity. We reveal design principles that underlie this complexity by mathematical modeling. Our proposed methodology of fitting model parameters to synchronization features at different entrainment protocols (e.g., varying thermo- or photoperiods) can be easily adapted to other systems of externally driven biological oscillators.

Limitations of the study

Although experimental observations can be reliably reproduced in case of the wild type frq^+ strain, the dynamical behavior of the long period frq^7 and short period frq^1 mutant can only be reproduced in up to $\approx 82\%$ of the T and x_T combinations (compare Figure S17). However, simulated dynamics of the frq^7 and frq^1 strain have been obtained by parameter changes as described in (Hong et al. (2008)). Because such studies focused on dynamics in constant darkness without considering entrainment characteristics, it would be interesting to further investigate in future studies whether other combinations of parameter changes could reproduce the constant darkness free-running periods and temperature entrainment dynamics at the same time.

STAR★METHODS

Detailed methods are provided in the online version of this paper and include the following:

- KEY RESOURCES TABLE
- RESOURCE AVAILABILITY
 - Lead contact
 - Materials availability
 - Data and code availability
- EXPERIMENTAL MODEL AND SUBJECT DETAILS
- METHOD DETAILS
 - Temperature cycles and race tube assays
 - Data analysis
 - Ordinary differential equations and kinetic parameters
 - Re-scaling of intrinsic period
 - Implementation of zeitgeber signal
 - Numerical simulations

SUPPLEMENTAL INFORMATION

Supplemental information can be found online at <https://doi.org/10.1016/j.isci.2021.103370>.

ACKNOWLEDGMENTS

This work was supported by the Japan Society for the Promotion of Science (JSPS) through grant number PE17780 and the German Research Foundation (DFG) through grant numbers SCHM3362/2-1, TRR186 (project number 278001972) and the CompCancer Graduate School (RTG2424). P.B. and C.S. acknowledge support from the Joachim Herz Stiftung.

AUTHOR CONTRIBUTIONS

MM, TR, HH and CS conceived and designed the study. CM performed experiments. PB, SG, CM, MM, TR, HH and CS analyzed the data. PB, SG and CS performed simulations. PB, AU and CS performed visualization of results. HH and CS wrote text. All authors revised and approved the manuscript.

DECLARATION OF INTERESTS

The authors declare no competing interests.

Received: April 30, 2021
Revised: September 1, 2021
Accepted: October 25, 2021
Published: November 19, 2021

REFERENCES

- Abraham, U., Granada, A.E., Westermarck, P.O., Heine, M., Kramer, A., and Herzl, H. (2010). Coupling governs entrainment range of circadian clocks. *Mol. Syst. Biol.* **6**, 438.
- Ananthasubramaniam, B., Schmal, C., and Herzl, H. (2020). Amplitude effects allow short jet lags and large seasonal phase shifts in minimal clock models. *J. Mol. Biol.* **27**, 3722–3737.
- Arnold, V. (1987). Geometrische Methoden in der Theorie der gewöhnlichen Differentialgleichungen (Birkhäuser Verlag).
- Aronson, B., Johnson, K., Loros, J., and Dunlap, J. (1994). Negative feedback defining a circadian clock: autoregulation of the clock gene *frequency*. *Science* **263**, 1578–1584.
- Aschoff, J. (1958). Tierische Periodik unter dem Einfluß von Zeitgebern. *Z. Tierpsychol.* **15**, 1–30.
- Bain, E., Millar, A., and Turner, M. (2004). The wild-type circadian period of *Neurospora* is encoded in the residual network of the null *frq* mutants. *J. Theor. Biol.* **229**, 413–420.
- Balanov, A., Janson, N., Postnov, D., and Sosnovtseva, O. (2009). Synchronization: From Simple to Complex (Springer-Verlag Berlin Heidelberg).
- Belden, W.J., Larrondo, L.F., Froehlich, A.C., Shi, M., Chen, C.H., Loros, J.J., and Dunlap, J.C. (2007). Dissecting the mechanisms of the clock in *neurospora*. *Gene Dev.* **21**, 1494–1505.
- Bergé, P., Pomeau, Y., and Vidal, C. (1984). Order within Chaos: Towards a Deterministic Approach to Turbulence (Hermann).
- Bordyugov, G., Abraham, U., Granada, A., Rose, P., Imkeller, K., Kramer, A., and Herzl, H. (2015). Tuning the phase of circadian entrainment. *J. R. Soc. Interf.* **12**, 20150282.
- Bradley, E., and Kantz, H. (2015). Nonlinear time-series analysis revisited. *Chaos: Interdiscip. J. Nonlinear Sci.* **25**, 097610.
- Brown, S.A., Zumbrunn, G., Fleury-Olela, F., Preitner, N., and Schibler, U. (2002). Rhythms of mammalian body temperature can sustain peripheral circadian clocks. *Curr. Biol.* **12**, 1574–1583.
- Bruce, V.G. (1960). Environmental entrainment of circadian rhythms. *Cold Spring Harbor Symp. Quant. Biol.* **25**, 29–48.
- Buhr, E.D., Yoo, S.H., and Takahashi, J.S. (2010). Temperature as a universal resetting cue for mammalian circadian oscillators. *Science* **330**, 379–385.
- Bünning, E., and Tazawa, M. (1957). Über den Temperatureinfluss auf die endogene Tagesrhythmik bei *Phaseolus*. *Planta* **50**, 107–121.
- Colot, H.V., Loros, J.J., and Dunlap, J.C. (2005). Temperature-modulated alternative splicing and promoter use in the circadian clock gene *frequency*. *Mol. Biol. Cell* **16**, 5563–5571.
- Crosthwaite, S.K., Loros, J.J., and Dunlap, J.C. (1995). Light-induced resetting of a circadian clock is mediated by a rapid increase in frequency transcript. *Cell* **81**, 1003–1012.
- De Caluwe, J., de Melo, J.R.F., Tosenberger, A., Hermans, C., Verbruggen, N., Leloup, J.C., and Gonze, D. (2017). Modeling the photoperiodic entrainment of the plant circadian clock. *J. Theor. Biol.* **420**, 220–231.
- Diegmann, J., Stück, A., Madeti, C., and Roenneberg, T. (2010). Entrainment elicits period aftereffects in *Neurospora crassa*. *Chronobiol. Int.* **27**, 1335–1347.
- Diekmann, C.O., and Bose, A. (2018). Reentrainment of the circadian pacemaker during jet lag: east-west asymmetry and the effects of north-south travel. *J. Theor. Biol.* **437**, 261–285.
- Diernfellner, A.C.R., Schafmeier, T., Mellow, M.W., and Brunner, M. (2005). Molecular mechanism of temperature sensing by the circadian clock of *Neurospora crassa*. *Gene Dev.* **19**, 1968–1973.
- Diernfellner, A., Colot, H.V., Dintsis, O., Loros, J.J., Dunlap, J.C., and Brunner, M. (2007). Long and short isoforms of *neurospora* clock protein *frq* support temperature-compensated circadian rhythms. *FEBS Lett.* **581**, 5759–5764.
- Dodd, A.N., Salathia, N., Hall, A., Kévei, E., Tóth, R., Nagy, F., Hibberd, J.M., Millar, A.J., and Webb, A.A.R. (2005). Plant circadian clocks increase photosynthesis, growth, survival, and competitive advantage. *Science* **309**, 630–633.
- Dovzhenok, A.A., Baek, M., Lim, S., and Hong, C.I. (2015). Mathematical modeling and validation of glucose compensation of the *Neurospora* circadian clock. *Biophys. J.* **108**, 1830–1839.
- Dunlap, J.C. (1999). Molecular bases for circadian clocks. *Cell* **96**, 271–290.
- Ermentrout, B. (2002). Simulating, Analyzing, and Animating Dynamical Systems: A Guide to XPPAUT for Researchers and Students (SIAM).
- Erzberger, A., Hampp, G., Granada, A.E., Albrecht, U., and Herzl, H. (2013). Genetic redundancy strengthens the circadian clock leading to a narrow entrainment range. *J. R. Soc. Interf.* **20130221**.
- Francois, P. (2005). A model for the *Neurospora* circadian clock. *Biophys. J.* **88**, 2369–2383.
- Froehlich, A.C., Liu, Y., Loros, J.J., and Dunlap, J.C. (2002). White collar-1, a circadian blue light photoreceptor, binding to the *frequency* promoter. *Science* **297**, 815–819.
- Fuhr, L., Abreu, M., Pett, P., and Relogio, A. (2015). Circadian systems biology: when time matters. *Comput. Struct. Biotechnol. J.* **13**, 417–426.
- Gardner, G.F., and Feldman, J.F. (1981). Temperature compensation of circadian period length in clock mutants of *Neurospora crassa*. *Plant Physiol.* **68**, 1244–1248.
- Glass, L., Guevara, M.R., Belair, J., and Shrier, A. (1984). Global bifurcations of a periodically forced biological oscillator. *Phys. Rev.* **29**, 1348–1357.
- Gonze, D., and Goldbeter, A. (2000). Entrainment versus chaos in a model for a circadian oscillator driven by light-dark cycles. *J. Stat. Phys.* **101**, 649–663.
- Gonze, D., Bernard, S., Waltermann, C., Kramer, A., and Herzl, H. (2005). Spontaneous synchronization of coupled circadian oscillators. *Biophys. J.* **89**, 120–129.
- Granada, A.E., Cambras, T., Diez-Noguera, A., and Herzl, H. (2011). Circadian desynchronization. *Interf. Focus* **1**, 153–166.
- Guevara, M.R., Glass, L., and Shrier, A. (1981). Phase locking, period-doubling bifurcations, and irregular dynamics in periodically stimulated cardiac cells. *Science* **214**, 1350–1353.
- Heltberg, M.L., Krishna, S., Kadanoff, L.P., and Jensen, M.H. (2021). A tale of two rhythms: locked clocks and chaos in biology. *Cell Syst.* **12**, 291–303.
- Hoffmann, K. (1969). Zum Einfluß der Zeitgeberstärke auf die Phasenlage der synchronisierten circadianen Periodik. *Z. für Vgl. Physiol.* **62**, 93–110.
- v. Holst, E. (1938). Über relative Koordination bei Säugern und beim Menschen. *Pflüger's Archiv für die gesamte Physiologie des Menschen und der Tiere* **240**, 44–59.
- Hong, C.I., Jolma, I.W., Loros, J.J., Dunlap, J.C., and Ruoff, P. (2008). Simulating dark expressions and interactions of *frq* and *wc-1* in the *Neurospora* circadian clock. *Biophys. J.* **94**, 1221–1232.
- Huang, G., Wang, L., and Liu, Y. (2006). Molecular mechanism of suppression of circadian rhythms by a critical stimulus. *EMBO J.* **25**, 5349–5357.
- Hurley, J.M., Loros, J.J., and Dunlap, J.C. (2016). The circadian system as an organizer of metabolism. *Fungal Genet. Biol.* **90**, 39–43.
- Hut, R.A., Paolucci, S., Dor, R., Kyriacou, C.P., and Daan, S. (2013). Latitudinal clines: an evolutionary view on biological rhythms. *Proc. Biol. Sci.* **280**, 20130433.

- Johnson, M.S. (1926). Activity and distribution of certain wild Mice in relation to Biotic Communities. *J. Mammal.* 7, 245–277.
- Konopka, R.J., and Benzer, S. (1971). Clock mutants of *Drosophila melanogaster*. *PNAS* 68, 2112–2116.
- Lakin-Thomas, P.L., Brody, S., and Coté, G.G. (1991). Amplitude model for the effects of mutations and temperature on period and phase resetting of the neurospora circadian oscillator. *J. Biol. Rhythms* 6, 281–297.
- Lee, K., Loros, J.J., and Dunlap, J.C. (2000). Interconnected feedback loops in the *Neurospora* circadian system. *Science* 289, 107–110.
- Larrondo, L.F., Olivares-Yañez, C., Baker, C.L., Loros, J.J., and Dunlap, J.C. (2015). Decoupling circadian clock protein turnover from circadian period determination. *Science* 347, 1257277.
- Lee, K., Dunlap, J.C., and Loros, J.J. (2003). Roles for WHITE COLLAR-1 in circadian and general photoperception in *Neurospora crassa*. *Genetics* 163, 103–114.
- Leloup, J.C., Gonze, D., and Goldbeter, A. (1999). Limit cycle models for circadian rhythms based on transcriptional regulation in *Drosophila* and *Neurospora*. *J. Biol. Rhythms* 14, 433–448.
- Liu, Y. (2003). Molecular mechanisms of entrainment in the *Neurospora* circadian clock. *J. Biol. Rhythms* 18, 195–205.
- Liu, Y., Garceau, N.Y., Loros, J.J., and Dunlap, J.C. (1997). Thermally regulated translational control of FRQ mediates aspects of temperature responses in the *Neurospora* circadian clock. *Cell* 89, 477–486.
- Liu, Y., Mellow, M., Loros, J.J., and Dunlap, J.C. (1998). How temperature changes reset a circadian oscillator. *Science*, 825–829.
- Loros, J.J., Denome, S.A., and Dunlap, J.C. (1989). Molecular cloning of genes under control of the circadian clock in neurospora. *Science*, 385–388.
- Maguire, S.E., Schmidt, P.S., and Sehgal, A. (2014). Natural populations of *Drosophila melanogaster* reveal features of an uncharacterized circadian property: the lower temperature limit of rhythmicity. *J. Biol. Rhythms* 29, 167–180.
- Mayer, W. (1966). Besonderheiten der circadianen Rhythmik bei Pflanzen verschiedener geographischer Breiten. *Planta* 70, 237–256.
- Mellow, M., Brunner, M., and Roenneberg, T. (1999). Assignment of circadian function for the *Neurospora* clock gene frequency. *Nature* 399, 584–586.
- Murayama, Y., Kori, H., Oshima, C., Kondo, T., Iwasaki, H., and Ito, H. (2017). Low temperature nullifies the circadian clock in cyanobacteria through Hopf bifurcation. *Proc. Natl. Acad. Sci. U S A* 114, 5641–5646.
- Pikovsky, A., Rosenblum, M., and Kurths, J. (2001). *Synchronization: A Universal Concept in Nonlinear Sciences* (Cambridge University Press).
- Pittendrigh, C.S., and Daan, S. (1976). A functional analysis of circadian pacemakers in nocturnal rodents. *J. Comp. Physiol.* 106, 223–252.
- Rensing, L., and Ruoff, P. (2002). Temperature effect on entrainment, phase shifting, and amplitude of circadian clocks and its molecular bases. *Chronobiology Int.* 19, 807–864.
- Roberts, S.K.d.F. (1960). Circadian activity rhythms in cockroaches. i. the free-running rhythm in steady-state. *J. Cell Comp. Physiol.* 55, 99–110.
- Roenneberg, T., Dragovic, Z., and Mellow, M. (2005). Demasking biological oscillators: properties and principles of entrainment exemplified by the *Neurospora* circadian clock. *PNAS* 102, 7742–7747.
- Rosato, E., Peixoto, A.A., Gallippi, A., Kyriacou, C.P., and Costa, R. (1996). Mutational mechanisms, phylogeny, and evolution of a repetitive region within a clock gene of *Drosophila melanogaster*. *J. Mol. Evol.* 42, 392–408.
- Ruoff, P., Vinsjevik, M., Monnerjahn, C., and Rensing, L. (2001). The goodwin model: simulating the effect of light pulses on the circadian sporulation rhythm of *Neurospora crassa*. *J. Theor. Biol.* 209, 29–42.
- Ruoff, P., Loros, J.J., and Dunlap, J.C. (2005). The relationship between FRQ-protein stability and temperature compensation in the *Neurospora* circadian clock. *Proc. Natl. Acad. Sci. U S A* 102, 17681–17686.
- Rémi, J., Mellow, M., and Roenneberg, T. (2010). A circadian surface of entrainment: varying t , τ , and photoperiod in *Neurospora crassa*. *J. Biol. Rhythms* 25, 318–328.
- Sargent, M.L., and Kaltenborn, S. (1972). Effects of medium composition and carbon dioxide on circadian oscillation in *Neurospora*. *Plant Physiol.* 50, 171–175.
- Sawyer, L.A., Hennessy, J.M., Peixoto, A.A., Rosato, E., Parkinson, H., Costa, R., and Kyriacou, C.P. (1997). Natural variation in a *Drosophila* clock gene and temperature compensation. *Science* 278, 2117–2120.
- Schafmeier, T., Haase, A., Kaldi, K., Scholz, J., Fuchs, M., and Brunner, M. (2005). Transcriptional feedback of *Neurospora* circadian clock gene by phosphorylation-dependent inactivation of its transcription factor. *Cell* 122, 235–246.
- Schmal, C., Leloup, J.C., and Gonze, D. (2014). Modeling and simulating the *Arabidopsis thaliana* circadian clock using XPP-AUTO. In *Plant Circadian Networks*, D. Staiger, ed. (Springer New York), pp. 337–358, number 1158 in *Methods in Molecular Biology*.
- Schmal, C., Myung, J., Herzel, H., and Bordyugov, G. (2015). A theoretical study on seasonality. *Front. Neurol.* 6, 94.
- Schmal, C., Herzel, H., and Myung, J. (2020). Clocks in the wild: entrainment to natural light. *Front. Physiol.* 11, 272.
- Schuster, H.G. (1994). *Deterministisches Chaos* (Wiley-VCH).
- Somers, D., Webb, A., Pearson, M., and Kay, S. (1998). The short-period mutant, *toc1-1*, alters circadian clock regulation of multiple outputs throughout development in *Arabidopsis thaliana*. *Development* 125, 485–494.
- Tseng, Y.Y., Hunt, S.M., Heintzen, C., Crosthwaite, S.K., and Schwartz, J.M. (2012). Comprehensive modelling of the *Neurospora* circadian clock and its temperature compensation. *PLOS Comput. Biol.* 8, 1–13.
- Upadhyay, A., Brunner, M., and Herzel, H. (2019). An inactivation switch enables rhythms in a *Neurospora* clock model. *Int. J. Mol. Sci.* 20, 2985.
- Upadhyay, A., Marzoll, D., Diernfellner, A., Brunner, M., and Herzel, H. (2020). Multiple random phosphorylations in clock proteins provide long delays and switches. *Sci. Rep.* 10, 22224.
- Wever, R. (1965). A mathematical model for circadian rhythms. In *Circadian Clocks*, J. Aschoff, ed., pp. 47–63.
- Wever, R. (1979). *The Circadian System of Man* (Springer-Verlag).
- Wheeler, D.A., Hamblen-Coyle, M.J., Dushay, M.S., and Hall, J.C. (1993). Behavior in light-dark cycles of *Drosophila* mutants that are arrhythmic, blind, or both. *J. Biol. Rhythms* 8, 67–94.
- Zimmerman, W.F. (1969). On the absence of circadian rhythmicity in *Drosophila pseudoobscura* pupae. *Biol. Bull.* 136, 494–500.

STAR★METHODS

KEY RESOURCES TABLE

REAGENT or RESOURCE	SOURCE	IDENTIFIER
Experimental models: Organisms/strains		
<i>Neurospora crassa</i> : bdA	Fungal Genetic Stock Center	FGSC #1858
<i>Neurospora crassa</i> : bd-frq1A	Fungal Genetic Stock Center	FGSC #2670
<i>Neurospora crassa</i> : bd-frq7A	Fungal Genetic Stock Center	FGSC #4898
Software and algorithms		
XPP-Aut	Ermentrout (2002)	http://www.math.pitt.edu/~bard/bardware/tut/start.html
Python 2.7.15		https://www.python.org
Astropy 2.0.16		https://www.astropy.org
Scipy 1.2.1		https://scipy.org

RESOURCE AVAILABILITY

Lead contact

Further information and requests for resources, reagents and code should be directed to and will be fulfilled by the lead contact, Christoph Schmal (christoph.schmal@hu-berlin.de).

Materials availability

This study did not generate new unique reagents.

Data and code availability

- All data reported in this paper will be shared by the lead contact upon request.
- Code generated during this study is available at GitHub: https://github.com/cschmal/NC_Temp_Entrainment
- Any additional information required to reanalyze the data reported in this paper is available from the lead contact upon request.

EXPERIMENTAL MODEL AND SUBJECT DETAILS

Three *Neurospora crassa* strains with different free running periods τ_{DD} in constant darkness were used in the present study: The standard laboratory strain *bd A 30-7* ($\tau = 22h$, denoted as *frq*⁺) the *frq*¹ strain ($\tau = 16h$) and the *frq*⁷ strain ($\tau = 29h$ and deficient in temperature compensation at low temperatures) (Sargent and Kaltenborn (1972); Loros et al. (1989)). Both *frq*¹ and *frq*⁷ derive from the *frq*⁺ strain but additionally carry a mutation in the *frq* gene (Loros et al. (1989)). They can be obtained from the Fungal Genetics Stock Center (Kansas City, KS, USA).

METHOD DETAILS

Temperature cycles and race tube assays

Temperature cycles were generated in customized incubators containing two integrated waterbaths that facilitated precise alternations between warming and cooling. Temperatures were thereby varied between 22°C and 27°C and *Neurospora* conidiation was assessed on race tubes filled with 10 ml of molten race tube media (2% Agar, 1X Vogel's solution, 0.5% Arginine, 1 ng/1 ml Biotin, no glucose). All tubes were inoculated and germinated for 24 h in constant light at 25°C before exposure to temperature cycles in darkness. Growth rates were marked at intervals under red light. Conidiation was then measured using densitometric analysis as previously described (Rémi et al. (2010)).

Data analysis

Neurospora conidiation patterns were transformed and normalized to densitometric intensities. Instantaneous phases were computed using the hilbert function from the scipy.signal library in python. Spectral analysis was performed after removal of the first 48h which were considered transient dynamics using the LombScargle method from the Astropy package. In cases where conidiation stopped before the end of the experiment run time, possibly due to medium limitations, corresponding time points were excluded from downstream analysis. Data were categorized as entrained or non-entrained according to three different criteria commonly used in the analysis of nonlinear dynamcis, namely the critical inspection of 1) raw time-series 2) phase-portraits and 3) spectra (Bergé et al. (1984); Schuster (1994); Erzberger et al. (2013)).

Ordinary differential equations and kinetic parameters

The evolution of the *Neurospora crassa* core clock dynamics follows equations

$$\frac{d[frq\ mRNA]}{dt} = k_1 \frac{[WC - 1_n]^2}{K + [WC - 1_n]^2} - k_4 [frq\ mRNA] \quad \text{(Equation 1a)}$$

$$\frac{d[FRQ_c]}{dt} = k_2 [frq\ mRNA] - (k_3 + k_5) [FRQ_c] \quad \text{(Equation 1b)}$$

$$\frac{d[FRQ_n]}{dt} = k_3 [FRQ_c] + k_{14} [FRQ_n : WC - 1_n] \quad \text{(Equation 1c)}$$

$$- [FRQ_n] (k_6 + k_{13} [WC - 1_n])$$

$$\frac{d[wc - 1\ mRNA]}{dt} = k_7 - k_{10} [wc - 1\ mRNA] \quad \text{(Equation 1d)}$$

$$\frac{d[WC - 1_c]}{dt} = \frac{k_9 [FRQ_c] [wc - 1\ mRNA]}{K_2 + [FRQ_c]} - (k_9 + k_{11} [WC - 1_c]) \quad \text{(Equation 1e)}$$

$$\frac{d[WC - 1_n]}{dt} = k_9 [WC - 1_c] - [WC - 1_n] (k_{12} + k_{13} [FRQ_n]) + k_{14} [FRQ_n : WC - 1_n] \quad \text{(Equation 1f)}$$

$$\frac{d[FRQ_n : WC - 1_n]}{dt} = k_{13} [FRQ_n] [WC - 1_n] - (k_{14} + k_{15}) [FRQ_n : WC - 1_n] \quad \text{(Equation 1g)}$$

as previously published (Hong et al. (2008)), using the nominal parameter set as given in Table 1 for a subsequent optimization. Dynamics of the long period frq^7 and the short period frq^1 strain are simulated by setting $k_5 = 0.15h^{-1}$ and $k_6 = 0.01h^{-1}$ or $k_3 = 0.15h^{-1}$, $k_5 = 0.4h^{-1}$ and $k_6 = 0.1h^{-1}$, respectively, as described in (Hong et al. (2008)).

Re-scaling of intrinsic period

Using vector notation we can rewrite Equations 1a, 1b, 1c, 1d, 1e, 1f, and 1g as $\frac{d\vec{x}}{dt} = \vec{f}(\vec{x})$ with $\vec{x} := ([frq\ mRNA], [FRQ_c], [FRQ_n], [wc - 1\ mRNA], [WC - 1_c], [WC - 1_n], [FRQ_n : WC - 1_n])^T$. Such autonomous dynamical systems with $\vec{f}(\vec{x})$ not explicitly depending on t , can always be rescaled in time. Defining a new variable $t' = c t$ with c being constant and using the chain rule

$$\frac{d\vec{x}}{dt} = \frac{d\vec{x}}{dt'} \frac{dt'}{dt} = \frac{d\vec{x}}{dt'} \frac{1}{c} \quad \text{(Equation 2)}$$

we can rewrite Equations 1a, 1b, 1c, 1d, 1e, 1f, and 1g as

$$\frac{d\vec{x}}{dt'} = c \vec{f}(\vec{x}). \quad \text{(Equation 3)}$$

Solutions of this equation are identical to those obtained from 1a, 1b, 1c, 1d, 1e, 1f, and 1g with the time axis being rescaled via a factor c . By this means we can freely choose the intrinsic free-running period τ under constant conditions as used during our optimization protocol underlying Figures 5B, S17A, and S17C.

Implementation of zeitgeber signal

To simulate entrainment in the Hong model, we chose a zeitgeber function with flexible period, thermo-period and amplitude (zeitgeber strength), i.e.

$$Z(t) = 1 + \frac{z_0}{\pi} \cdot \arctan \left(s \cdot \mu \left(\cos \left(\frac{2\pi t}{T} \right) - \cos(\pi x) \right) \right) \quad (\text{Equation 4})$$

similar to what has been described in (Schmal et al. (2015)). Here, z_0 is the zeitgeber strength, s is the steepness of the function, T is the period, x is the thermoperiod and $\mu = \frac{T}{2\sin(\pi x)}$ defines the slope at the switch points so that $|Z'(t)|_{t=\frac{z_0}{2}} = z_0 \cdot s$. In this study we set $s = 100$. Based on our bifurcation analysis and on earlier

works demonstrating the importance of *frq* transcription and translation for temperature entrainment (Liu et al. (1997; 1998)), we chose to modulate the *frq* transcription rate k_1 to investigate entrainment in the *Hong model*. Note that *frq* transcription rate k_1 and *frq* translation rate k_2 show similar bifurcation patterns with a positive effect on the amplitude and little to no effect on the period and could thus both be used to implement entrainment from a theoretical perspective. Modulating the *frq* transcription rate k_1 with $Z(t)$ gives

$$\frac{d[\textit{frq mRNA}]}{dt} = Z(t) \cdot k_1 \frac{[WC - 1_n]^2}{K + [WC - 1_n]^2} - k_4 [\textit{frq mRNA}] \quad (\text{Equation 5})$$

while, alternatively, modulating *frq* translation rate k_2 as used in Figure S16 gives

$$\frac{d[FRQ_c]}{dt} = Z(t) \cdot k_2 [\textit{frq mRNA}] - (k_3 + k_5) [FRQ_c]. \quad (\text{Equation 6})$$

Numerical simulations

Simulations were performed using the scientific python environment. Ordinary differential equations were solved using the `odeint` function from the `scipy.integrate` module with a time step of $\Delta t = 0.1$. Simulations were performed for 200 zeitgeber cycles of which the first 100 cycles were excluded to avoid transient effects that might arise at the vicinity of the Arnold tongue.

Determination of the entrained state and order of synchronization within simulated dynamics has been determined as previously described (Schmal et al. (2015)). Bifurcation analysis was performed using XPP-Auto (Ermentrout (2002); Schmal et al. (2014)) as well as brute force simulations.